Proceedings of the International Gas Turbine Congress 2003 Tokyo
November 2-7, 2003

IGTC2003Tokyo TS-049

Numerical and Experimental Investigation of the Unsteady Flow Field in a Transonic Centrifugal Compressor

Hartmut KRAIN[1] and Chunill HAH[2]

[1] German Aerospace Center (DLR)
Linder Hoehe, D-51147 Koeln, Germany
FAX: ++49/2203/64395, E-mail: hartmut.krain@dlr.de
[2]NASA Glenn Research Center, USA

ABSTRACT

An experimental and numerical study was performed to investigate unsteady flow fields inside the vaneless and vaned diffuser areas of a high-pressure-ratio, transonic, centrifugal compressor. The compressor stage was designed as part of a program to develop a highly efficient, transonic, centrifugal compressor stage with a pressure ratio of 5.7. The rotor tip speed is 586 m/sec. at the design rotor speed. The vaned diffuser has a relatively small height of 9 mm with an exit radius ratio of 1.5. An experimental investigation of the flow field inside the compressor was carried out with a laser two-focus velocimeter developed at DLR. Unsteady flow measurements were taken at 32 instantaneous impeller positions. To understand detailed unsteady flow structures inside the vaned diffuser area, unsteady, viscous, three-dimensional flow analyses were conducted for the impeller/diffuser stage. The calculated flow fields represent the measurements very well. Both the measurements and the calculations show high unsteadiness in the flow field near the hub at the diffuser inlet area. The unsteadiness decays rapidly as the flow enters the vaned diffuser area, suggesting that a steady impeller/diffuser calculation procedure might calculate the time-averaged flow field fairly well for this type of flow.

INTRODUCTION

Centrifugal compressors are widely used both in stationary and aircraft applications. The current design trends in centrifugal compressors are to increase stage loading and to reduce the overall machine size. These requirements result in designs with transonic flows at the impeller and diffuser inlet areas. Centrifugal compressors with high pressure ratios are designed with vaned diffusers to obtain higher pressure recovery. The unsteady transonic flow structure in the region between the impeller exit and the diffuser inlet are believed to impact the operating range and the aerodynamic efficiency significantly. However, the flow physics in this area are not well understood at high speed.

A collaborative research program between DLR, Germany and NASA, U.S. has been conducted to advance the current understanding of the flow physics inside a high-pressure-ratio, centrifugal compressor. Extensive experimental studies with state-of-the-art measurement techniques were conducted in a high-pressure-ratio, centrifugal compressor (Eisenlohr et al., 1998; Hah and Krain, 1999; Krain et al., 1995; Krain and Hoffman, 1998; Krain, 1999; Krain et al., 2001). In parallel, steady and unsteady numerical studies were conducted to validate CFD codes and to investigate detailed flow structures (Hah, 1987; Hah and Wennerstrom, 1991; Maerz et al., 2002).

In the following section, the test rig and measurement techniques for the current unsteady flow investigation are described. This is followed by an explanation of the numerical procedures used for the three-dimensional, viscous, unsteady flow calculations. Numerical results are then compared with measurements. Finally, the calculated flow fields are used along with the measurements to study the flow structure.

Manuscript Received on May 6, 2003

TEST RIG AND INSTRUMENTATION

The DLR transonic centrifugal compressor test rig was used for carrying out the tests on the vaned diffuser. Figure 1 displays a meridional view of the slightly diagonal stage (13 degrees from radial). The main rig specifications are listed in Table 1. Due to the diagonal diffuser section, the diffuser geometry is completely three-dimensional. Figure 2 shows a photo of the open stage. The test facility is mainly suitable for testing rotors with high tip speeds and high pressure ratios. The overall stage dimensions are rather small. On the one hand, this ensures low energy consumption, which is important for long-term laser measurement campaigns. On the other hand, accessibility for the measurement systems is somewhat difficult.

Table 1 Test rig specifications.

Maximum power input	1500 kW
Maximum shaft speed	60,000 rpm
Maximum rotor tip speed	700 m/s
Maximum pressure ratio	9.5:1
Maximum flow rate	3.5 kg/s
Rotor tip diameter	250 mm
Stage diameter	600 mm
Powered by	2 DC motors

The compressor stage under consideration consists of a backswept, high-specific-speed impeller (Ns=105) and a vaned diffuser. The main design parameters of the overall stage equipped with the vaned diffuser are given in Table 2. At design speed the rotor runs with transonic inlet conditions; i.e. the relative rotor tip Mach number is supersonic and the flow conditions in the hub inlet region of the rotor are subsonic. The absolute Mach number in the vaned diffuser inlet region is also supersonic, which will be examined in more detail later on.

Previous steady measurements and calculations at the design speed revealed supersonic flow conditions at the rotor tip leading edge with a maximum relative Mach number of 1.4 (Eisenlohr et al., 1998; Hah and Krain, 1999; Krain et al., 1995; Krain et al., 2001). Unsteady measurements inside the diffuser were carried out with the laser-two-focus velocimeter available at DLR (Schodl, 1989). This technique was previously used for extensive rotor measurements and is most suitable for turbomachinery applications if high speeds and strong velocity gradients are present, as in transonic compressors with shocks (Krain and Hoffman, 1998; Krain, 1999).

Table 2 Stage design data.

Rotor shaft speed	50,000 rpm
Mass flow rate	2.55 kg/s
Rotor blade number	13+13
Rotor leading hub radius	30 mm
Rotor leading edge tip radius	78 mm
Rotor exit radius	112 mm
Rotor exit blade height	8.7 mm
Rotor exit blade angle	52 deg.
Rotor exit tip speed	586 m/s
Rotor inlet tip Mach number	1.3 (relative)
Diffuser blade number	23
Diffuser inlet/rotor exit radius ratio	1.15
Diffuser exit/rotor exit radius ratio	1.5

The measurement grid used on blade-to-blade planes for the laser measurements is shown in Fig.3. The 3D grid consists of four measurement planes located on constant radii (M1-M4) and a fifth plane that coincides with the diffuser throat (M5). Plane 1 is located in the middle of the vaneless space, plane 2 is just behind the diffuser leading edge, and plane 4 is positioned close to the vaned diffuser passage exit. Plane 3 is located half way between the vaned diffuser inlet and the vaned diffuser exit. At each plane, five measurement points equally spaced from the pressure side to suction side were selected to resolve the flow field. From hub to shroud, measurements were taken at 5 channel depths positioned at 10, 30, 50, 70 and 90% of channel height. In total, measurements were taken at 5X5X5 grid points. At each of these grid points, measurements were taken at 32 different impeller positions from which the unsteady flow character was found. The 32 measurements were triggered with the rotor blade frequency in such a way that the flow field is representative of two rotor flow passages adjacent to a splitter blade. Thus, differences resulting from different flow patterns caused by the rotor splitter blades were taken into account. The measured flow field is very complex and the flow character found at the diffuser mid span does not represent a diffuser mean flow condition. This is mainly due to the highly distorted flow discharged by the rotor that generates significantly different diffuser inlet flow conditions across the relatively small diffuser height (Krain, 1999). In general this results in a diffuser inlet flow with high positive incidence directed toward the diffuser pressure side in the shroud region and with negative incidence in the hub area.

NUMERICAL PROCEDURES

A numerical investigation was performed to examine detailed unsteady flow structures in the diffuser area. A three-dimensional Navier-Stokes code that has been tested for a wide variety of steady and unsteady turbomachinery flows (Hah, 1987; Hah and Wennerstrom, 1991; Maerz et al., 2002) was applied for the current problem. A third-order accurate interpolation scheme is used for the spatial discretization of the convection terms and central differencing is used for the diffusion terms. A modified two-equation model is used for the turbulence closure. The computational grid is shown in Fig. 4. A sliding overlapped grid interface is used to transmit flow variables between the impeller and the diffuser zones. The stage is composed of 13 impeller blades with a splitter in each passage and 23 diffuser blades. The primary objective of the current numerical analysis is to characterize the nature of unsteady flow structures in the diffuser area. To reduce necessary computational resources, the number of diffuser vanes was increased to 26. Consequently, unsteady flow analyses were performed for the flow in one impeller passage and two rescaled diffuser passages. For the investigated flow regime in the current centrifugal compressor stage, this scaling of the vaned diffuser is believed to have little effect on the study of the unsteady flow interaction.

The grid consists of 40 nodes in the blade-to-blade direction, 36 nodes in the spanwise direction, and 260 nodes in the streamwise direction. Six nodes are located between the blade tip and the casing to discretize the impeller tip clearance. Approximately 10 impeller rotations were required to obtain a periodic unsteady flow solution at each operating condition.

At the inlet of the computational domain, total pressure, total temperature, and two velocity components were specified. At the domain exit, static pressure was specified on the casing. Non-reflecting boundary conditions were applied. The computation was carried out on an SGI Origin 300 Workstation. Each operating condition required approximately 40 wall clock hours of computing.

RESULTS AND DISCUSSION

Measured and calculated stage performance maps at the design rotor speed of 50,000 rpm are shown in Fig. 5. Operating conditions where laser measurements were performed are marked by squares and those where numerical analyses were performed are marked by circles. The design point is at a mass flow rate of 2.55 kg/sec. and a total-to-total pressure ratio of 5.7:1. The numerical analyses predicted slightly lower adiabatic efficiency values than the measurements. However, the calculated pressure rise is in good agreement with the measured values.

Figure 6 shows measured and calculated mid-span velocity vectors at the design flow condition at four equally spaced impeller/diffuser relative positions during 1/13 of an entire impeller rotation. Computed vectors are shown at only a few computational nodes for clarity. Both the measured and calculated results show that the flow has negative incidence at the diffuser leading edge and that a low momentum area develops on the pressure side near the trailing edge. In Fig. 7, calculated velocity vectors at design condition at all time steps during 1/13 of an impeller rotation are plotted simultaneously to illustrate the degree of unsteadiness in the flow field. Significant unsteadiness can be seen at the diffuser inlet, but it quickly decays so that the flow becomes almost steady by the time it enters the diffuser passage.

Measured and calculated mid-span Mach number distributions at the design flow condition are shown in Fig. 8. The measured Mach number was calculated with the assumption of constant total temperature inside the diffuser. The measured and calculated values agree very well with each other, considering the various assumptions used to obtain them. The shape of the instantaneous Mach number distribution does not change significantly during operation since most of the unsteadiness occurs near the impeller exit. At this operating condition, a supersonic flow region extends from the impeller exit to the diffuser throat. No pronounced shock wave forms near the diffuser inlet area at this operating condition.

Figures 9 and 10 show measured and calculated instantaneous Mach number distributions near the hub and shroud, respectively, at the design condition. Corresponding calculated velocity vectors at all time steps are shown in Fig. 11. Near the shroud, the supersonic region extends upstream of the diffuser inlet, while near the hub, it extends further downstream into the diffuser passage. The instantaneous velocity vectors in Fig. 11 explain the trend shown in Figs. 9 and 10. The flow incidence angle is positive near the shroud, but negative near the hub. Velocity vectors in Fig. 11 indicate that unsteadiness is greater near the hub than near the shroud, because the impeller exit velocity profile has a more pronounced jet/wake structure near the hub than at the shroud (Hah and Krain [1999]).

Figure 12 shows calculated mid-span Mach number distributions for the two off-design operating conditions at four impeller/diffuser positions. Calculated off-design velocity vectors at all time steps are shown in Fig. 13. At the near-choke condition, the supersonic flow region extends into the diffuser passage. At the near-stall condition, the flow incidence at the diffuser leading edge increases and the supersonic flow region moves upstream. Also at the near-stall condition, decreased unsteadiness is observed in the velocity vectors. Again, this is due to the less pronounced jet/wake structure at mid-span

Figure 14 compares measured and calculated spanwise distributions of flow angle at measurement plane M1 for four impeller/diffuser positions at the design operating condition. Maxima and minima of the unsteady values at each spanwise location are illustrated by dashed lines for the measurements and solid lines for the calculations. The agreement between the measured and calculated flow angles is quite good, considering the complexity of the flow field and the various assumptions involved in both the experimental and the numerical procedures. Near the shroud, the numerical analysis predicts a flow angle roughly 5 degrees higher than the measurements. A variation of roughly 15 degrees in flow angle is observed on average during operation. A large change in flow angle from hub to shroud, on the order of 30 degrees, is observed at all impeller positions. The span of the diffuser is 9 mm, and the change of flow angle over this short span seems significant for impeller/diffuser matching.

CONCLUDING REMARKS

Experimental and numerical studies were performed to characterize unsteady flow fields in the vaned diffuser area of a high-pressure-ratio, centrifugal compressor. A laser two-focus technique was used for the experimental study while a three-dimensional unsteady Navier-Stokes procedure was applied for the numerical study. Both the measurements and the calculations show that high unsteadiness occurs, primarily in the vaneless area, and that the unsteadiness decays very rapidly as the flow moves downstream. The flow becomes almost steady near the exit of the diffuser. The unsteadiness is higher near the hub area than near the shroud area. Large variations in the incoming flow are observed from hub to shroud, which creates a challenge for impeller/diffuser matching. For the current stage, further design modifications seem necessary in order to improve the performance characteristics. The numerical procedure calculates the measured steady and unsteady flow fields very well. The current generation of numerical tools can be effectively applied to the design of such high pressure-ratio centrifugal compressors, reducing hardware tests during engine development.

REFERENCES

Eisenlohr, G., Dalbert, P., Krain, H., Pröll, H., Richter, F. A., and Rohne, K. H. 1998, "Analysis of the Transonic Flow at the Inlet of a High Pressure Ratio Centrifugal Impeller," ASME Paper 98-GT-24.

Hah, C., 1987, "Navier-Stokes Calculation of Three-Dimensional Compressible Flow Across a Cascade of Airfoils with an Implicit Relaxation Method," *AIAA Journal of Propulsion and Power*, Vol. 3, pp. 415-423.

Hah, C., and Krain, H., 1999, "Analysis of Transonic Flow Fields Inside a High Pressure Ratio Centrifugal Compressor at Design and Off Design Conditions," ASME Paper 99-GT-446.

Hah, C., and Wennerstrom, A. J., 1991, "Three-Dimensional Flow Fields Inside a Transonic Compressor with Swept Blades," *ASME Journal of Turbomachinery*, Vol. 113, No. 1, pp. 241-251.

Krain, H., Hoffmann, B., and Pak, H., 1995, "Aerodynamics of a Centrifugal Impeller with Transonic Inlet Conditions," ASME Paper 95-GT-79.

Krain, H., and Hoffmann, B., 1998, "Flow Physics in High Pressure Ratio Centrifugal Compressors," ASME Summer Meeting 1998, FEDSM98-4853.

Krain, H., 1999 "High Pressure Ratio Centrifugal Compressor with Transonic Flow," 3rd ASME/JSME Eng. Conference, FEDSM99-7801.

Krain, H., Karpinski, G., and Beversdorff, M., 2001, "Flow Analysis in a Transonic Centrifugal Compressor Rotor Using 3-Component Laser Velocimetry," ASME Paper 2001-GT-0315.

Maerz, J., Hah, C., and Neise, W., 2002, "An Experimental and Numerical Investigation into the Mechanisms of Rotating Instability," *ASME Journal of Turbomachinery*, Vol. 124, No. 3, pp. 367-375.

Schodl, R., 1989, "Measurement Techniques in Aerodynamics," VKI Lecture Series 1989- 05.

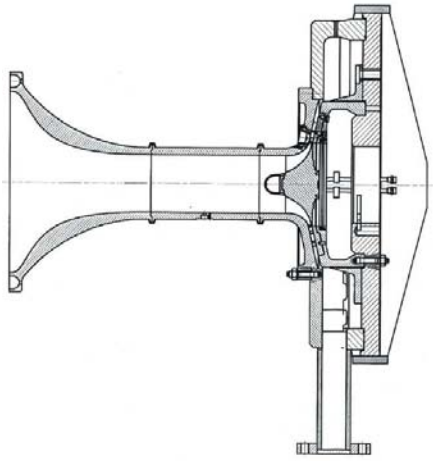

Figure 1. Meridional view of DLR transonic centrifugal compressor test rig.

Figure 2. Photo of the open stage with backswept rotor and vaned diffuser.

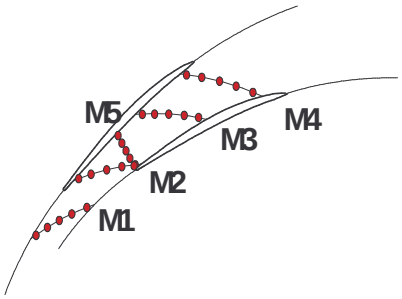

Figure 3. Measurement grid for vaned diffuser laser measurements.

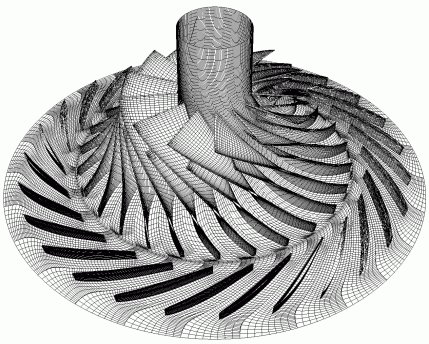

Figure 4. Computational grid for numerical analyses.

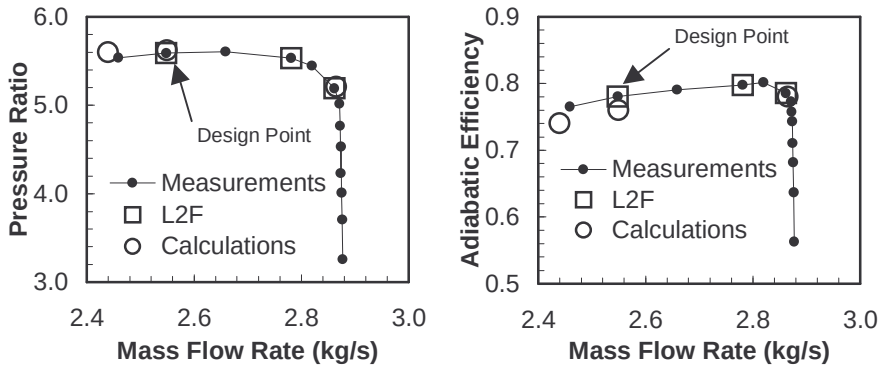

Figure 5. Measured and calculated performance maps at design rotor speed of 50,000 rpm.

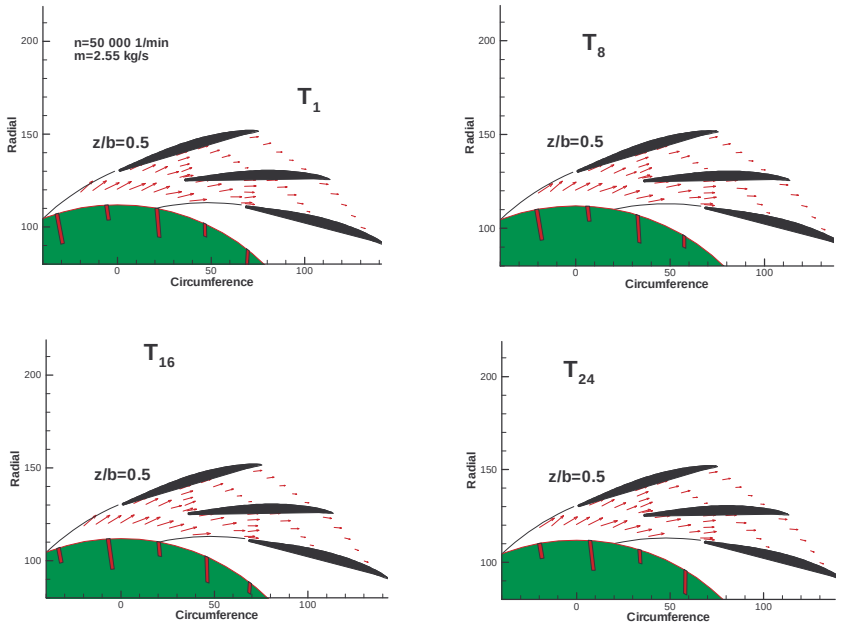

(a) measurements

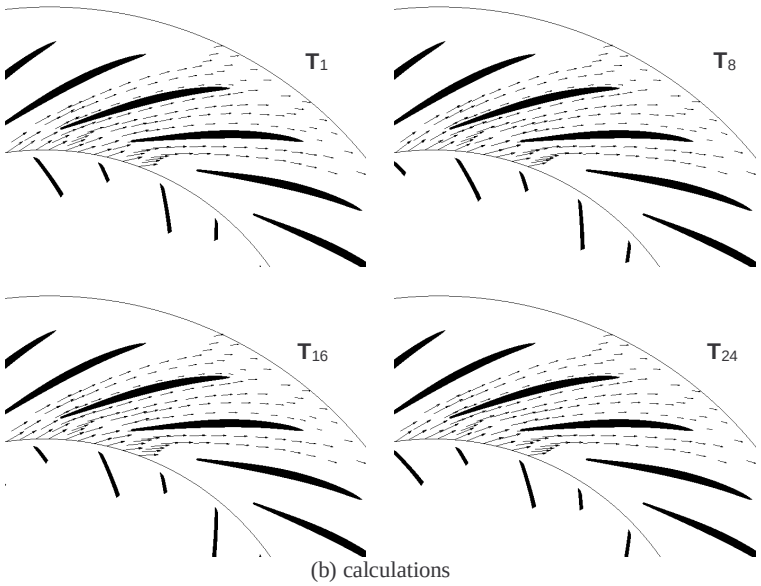

(b) calculations

Figure 6. Measured and calculated mid-span velocity vectors at design flow condition and 4 different impeller/diffuser positions.

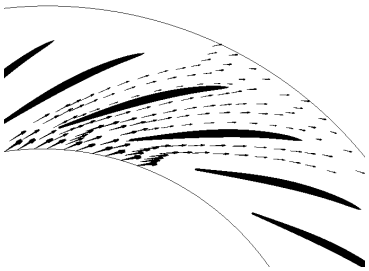

Figure 7 Calculated mid-span velocity vectors at all time steps during 1/13 of an impeller rotation.

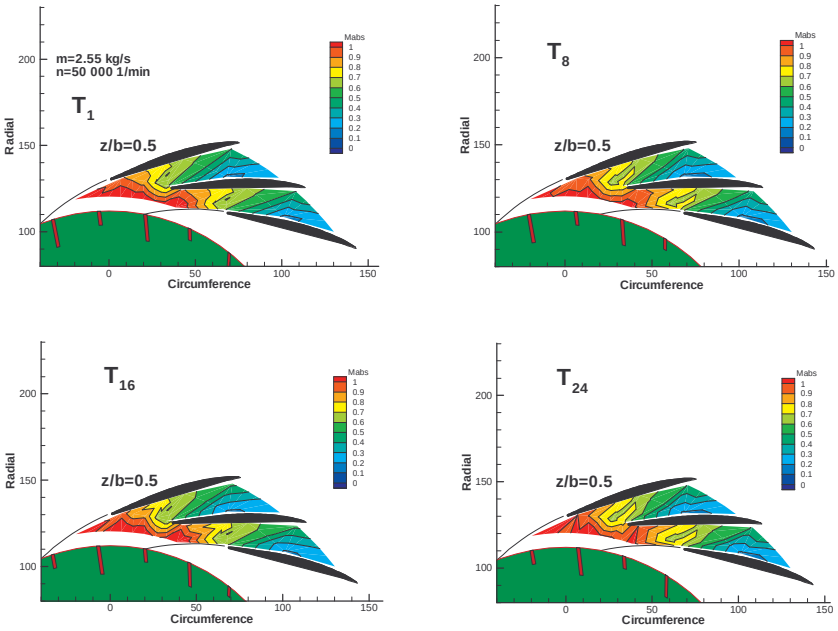

(a) measurements

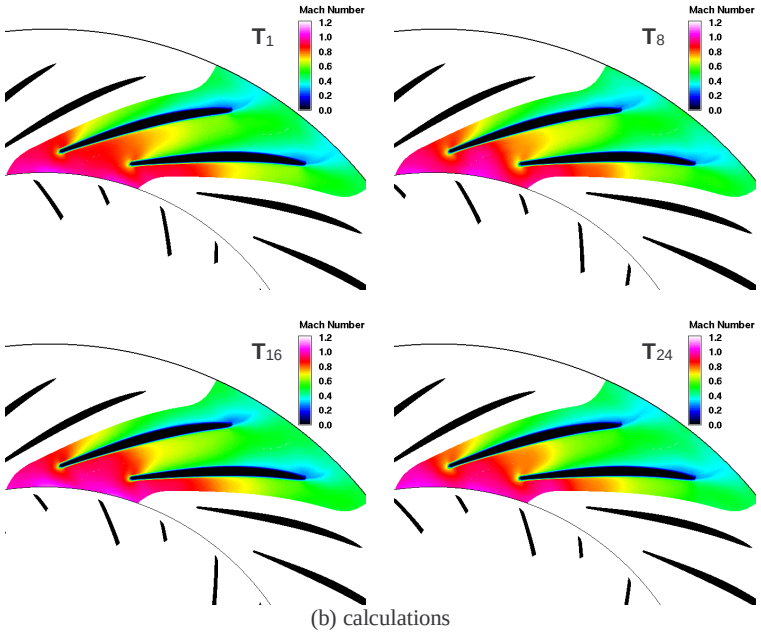

(b) calculations

Figure 8 Measured and calculated mid-span Mach number at design flow condition and 4 different impeller/diffuser positions.

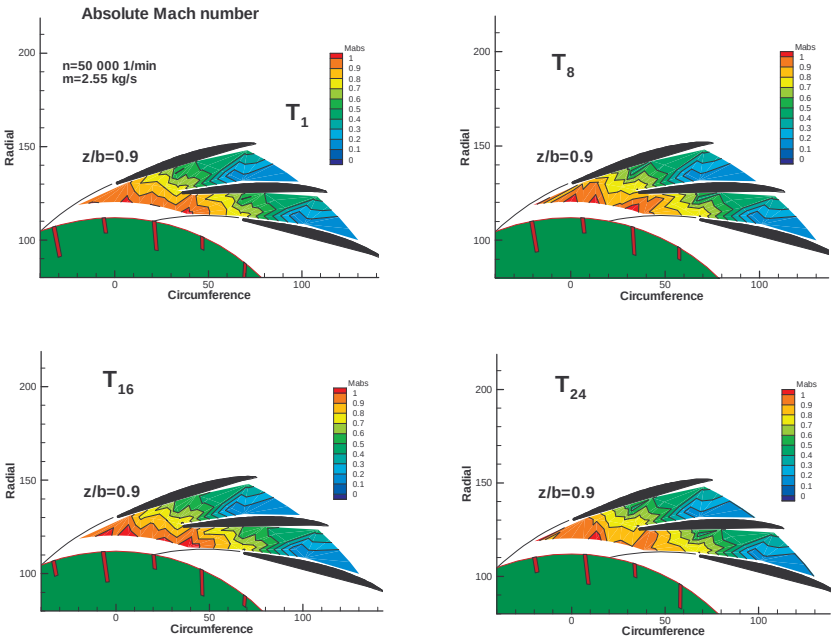

(a) measurements

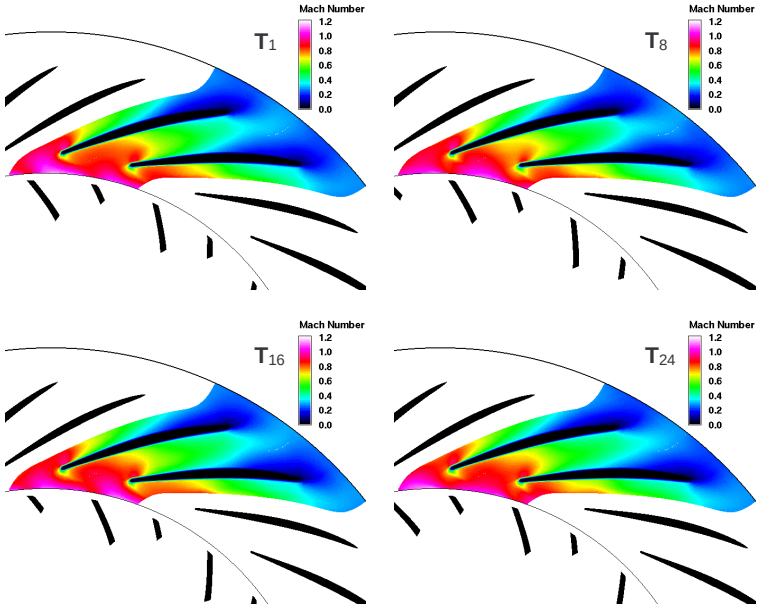

(b) calculations

Figure 9 Measured and calculated Mach number near hub at design condition and 4 different impeller/diffuser positions.

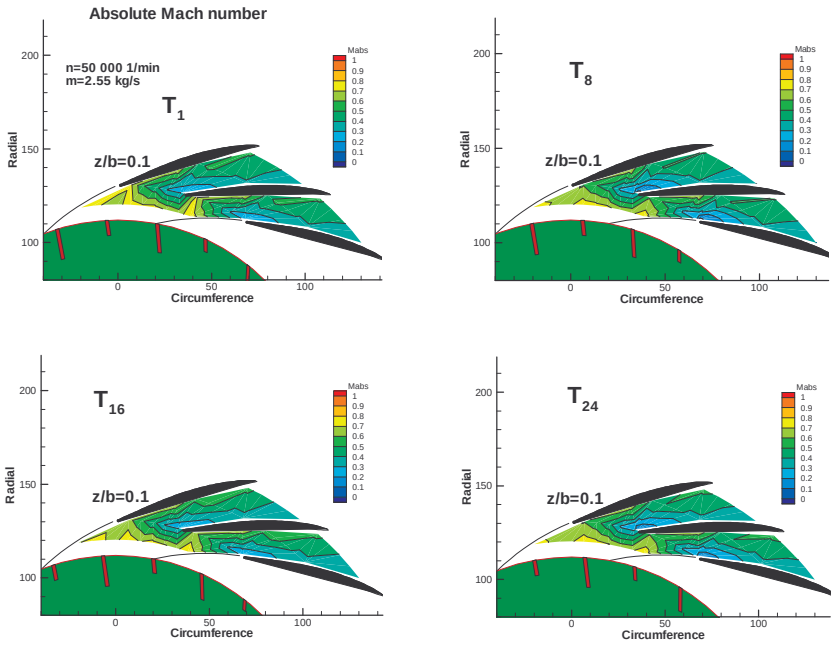

(a) measurements

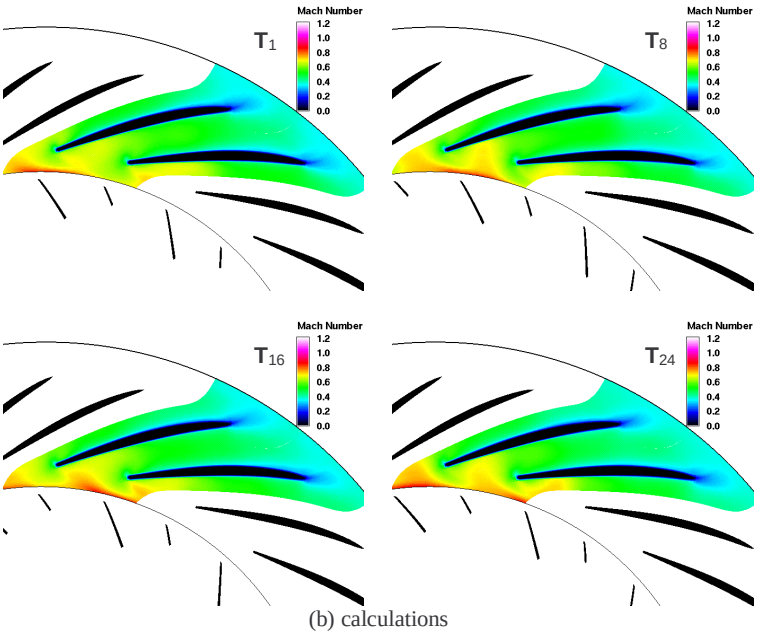

(b) calculations

Figure 10 Measured and calculated Mach number near shroud at design condition and 4 different impeller/diffuser positions.

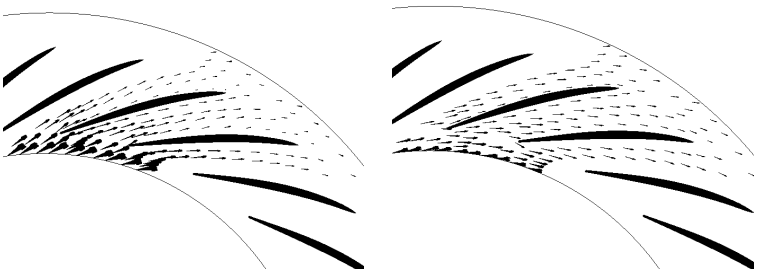

(a) near hub (b) near shroud

Figure 11 Calculated velocity vectors at design condition at all time steps during 1/13 of an impeller rotation.

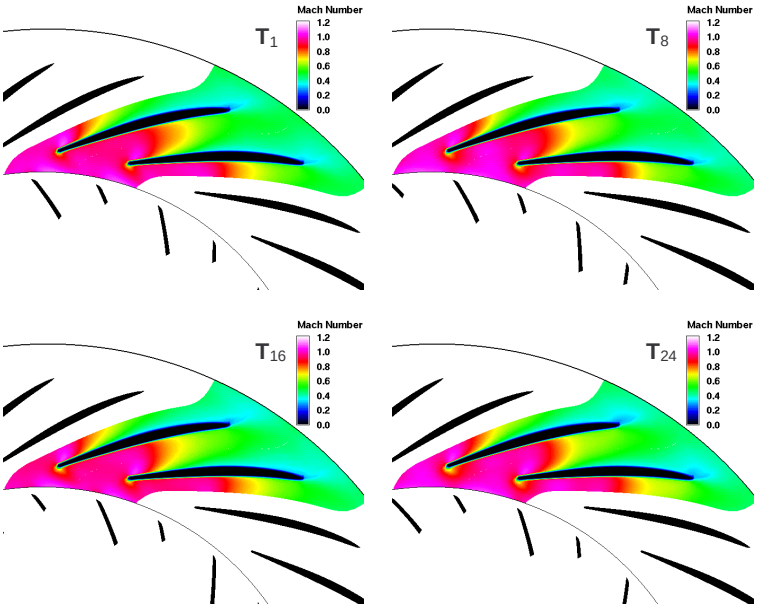

(a) near choke

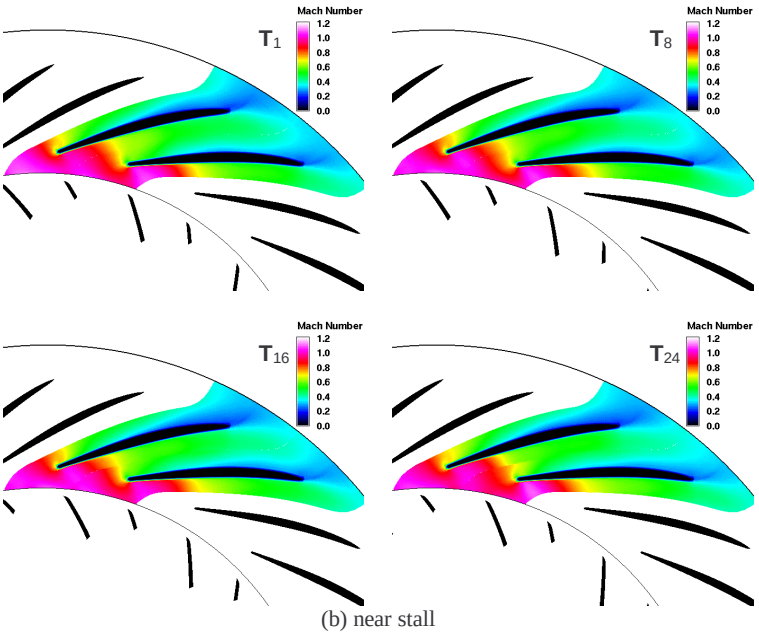

(b) near stall

Figure 12 Calculated mid-span Mach number at off-design flow conditions and 4 different impeller/diffuser positions.

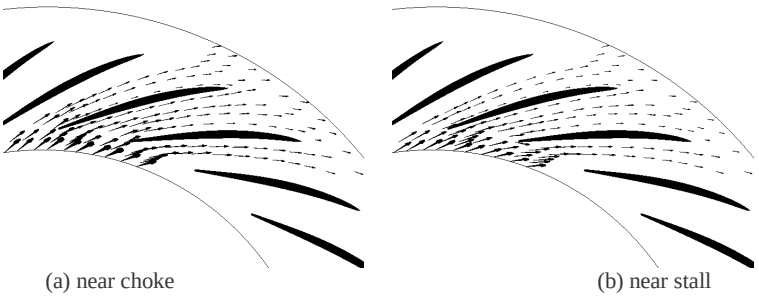

(a) near choke (b) near stall

Figure 13 Calculated mid-span velocity vectors at all time steps at off-design flow conditions.

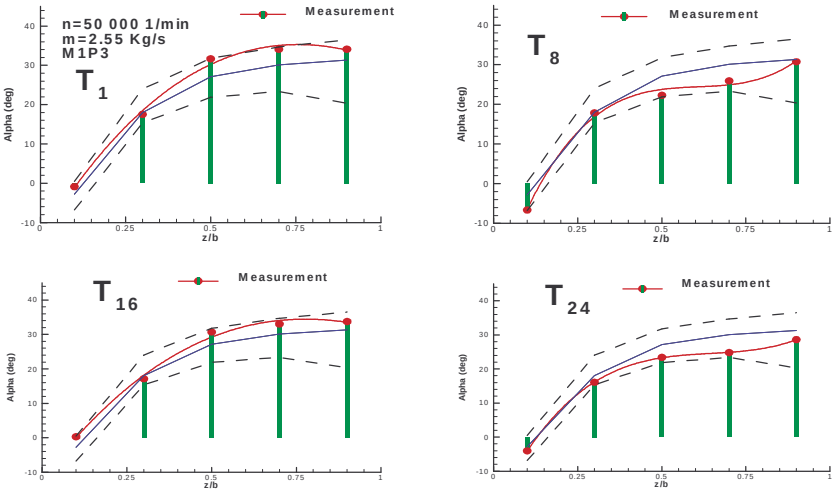

(a) measurements

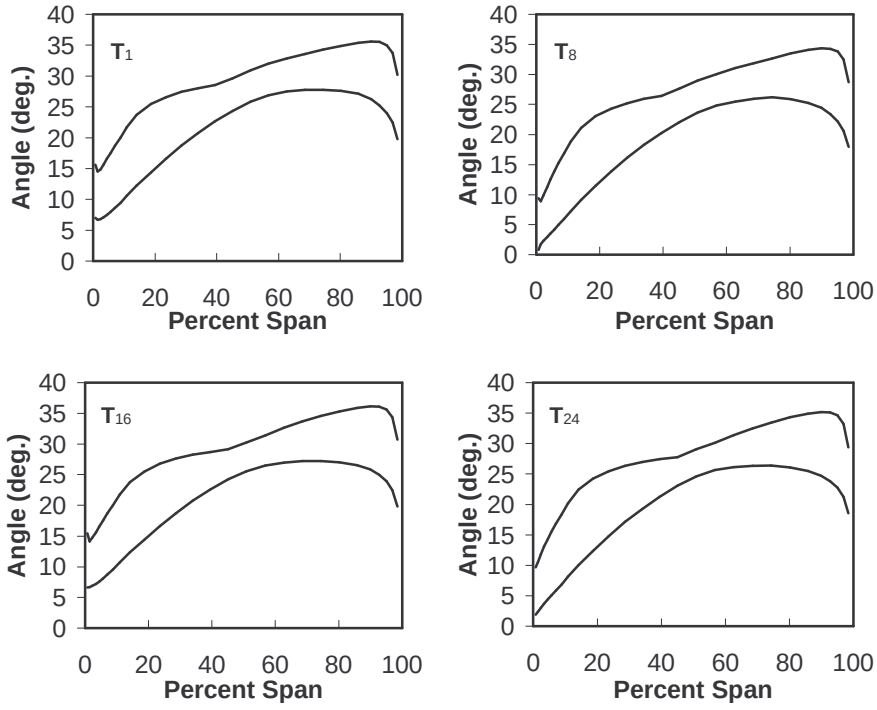

(b) calculations

Figure 14 Measured and calculated spanwise flow angle distributions at M1 and design condition at 4 different impeller/diffuser positions.